Fuel 292 (2021) 120396

Contents lists available at ScienceDirect

Fuel

journal homepage: www.elsevier.com/locate/fuel

Full Length Article

Specific heat capacity of wildland foliar fuels to 434 °C

Charles R. Boardman [a,*], Mark A. Dietenberger [a], David R. Weise [b]

[a] Building and Fire Sciences, Forest Products Laboratory, USDA Forest Service, Madison, WI 53726, United States
[b] Fire and Fuels Program, PSW Research Station, USDA Forest Service, Riverside, CA 92507, United States

ARTICLE INFO

Keywords:
Heat capacity
Fire modeling
Pyrolysis
Differential scanning calorimetry
Thermal analysis
Foliar fuels

ABSTRACT

Specific heat capacity of eleven live foliar fuels from the southeastern United States was measured to 434 °C using differential scanning calorimetry to improve the modeling of prescribed fire behavior. Techniques which allow measurement of the standard heat capacity, excluding the effects of heat of reaction, were refined. Specific heat of leaves increased with temperature until the onset of pyrolysis. Once pyrolysis began, the specific heat became nearly constant. We present a simple model, suitable for incorporation in computer simulations, which captures this functional shape. This model approach could be applied to other foliar fuels if the chemical composition is known. Measurement of standard heat capacity was used to estimate effective heat of reaction given the measurements of total heat flow which included heat of reaction. For all foliar fuels studied, effective heat of reaction was found to be mildly exothermic between 220 and 350 °C.

1. Introduction

A research project aiming to improve the modeling of prescribed fire behavior was undertaken to support management of wildlands in the southeastern United States [1]. As part of this effort, material properties were needed as inputs for physics-based fire models. Building upon the characterization of fuels previously advanced by Hough [2] and Susott [3], here, we focus on techniques for measuring the specific heat capacity of the leaves from several common wildland plant species native to the southern United States.

Specific heat capacity (C_p) is an intensive[1] material property defined as the amount of heat energy q (J) required to raise the temperature of one gram of material (mass, m) (g) one degree Kelvin (temperature, ΔT) (K), per Eq. (1).

$$C_p = q/(m \cdot \Delta T) \quad (1)$$

C_p is one of many material properties used when modeling both wildfires and prescribed fires and is necessary to describe the balance between "heat-source" and "heat-sink" properties of fuels [4]. Susott [3] noted that a fuel's heat-source (exothermic) characteristics originate from the combustion of vaporized fuel and pyrolyzates while the heat-sink (endothermic) characteristics are a function of the total energy required to produce those vaporized fuels and effect pyrolysis. Heat of combustion is the total heat released (heat-source) from a material during combustion. Heat capacity and chemical heat of reaction contribute to the total energy flow into (heat-sink) a material as it heats up, and undergoes pyrolysis, phase changes, and chars. These processes occur simultaneously, making determination of specific heat capacity above 200 °C challenging to obtain.

1.1. Background

While the importance of living fuels for modeling wildland fire spread has been recognized for over a century [5], early physical models of fire spread focused on dead fuels such as leaf litter and wood, and applied the specific heat of wood to all fuels [6]. Various thermal properties for a limited number of forest fuels have been determined [7,8], but specific heat has been largely ignored for foliar material. There are several studies that have determined the heat content (or heat of combustion) of wildland fuels using various types of calorimetry [2,9–14]. The change in heat of combustion seasonally has also been examined [15,16] and linked to changes in the composition of the foliage which occur during the annual growth cycle. The current operational fire spread model used in the United States [4] recognizes seasonal and species-specific differences observed in live fuels through an increased heat of combustion [17,18] associated with the presence of volatile compounds [19–21].

Investigation into live fuel heat-sink properties is limited. The

* Corresponding author.
E-mail addresses: charles.r.boardman@usda.gov (C.R. Boardman), mark.a.dietenberger@usda.gov (M.A. Dietenberger), david.weise@usda.gov (D.R. Weise).

[1] An intensive property is a bulk property, i.e. it does not depend on the amount of the material.

https://doi.org/10.1016/j.fuel.2021.120396
Received 8 December 2020; Received in revised form 29 January 2021; Accepted 1 February 2021
Available online 21 February 2021
0016-2361/Published by Elsevier Ltd.

specific heat capacity of vegetable material was previously determined [22] but the validity of applying these values to foliage of woody plants is unknown. Susott [3] used differential scanning calorimetry (DSC) to measure the total heat required to change the temperature of four common woody wildland fuels, two dead foliar fuels, and one green foliar fuel from 25 °C to 500 °C. This total heat included the specific heat capacity as well as the heat from other physical processes, such as heat of reaction. Susott converted the total heat into the mathematical form of specific heat using the initial sample mass and DSC heating rate (K/s). We refer to this measure as the total specific heat capacity, C_{total}. The complexity of C_{total} as a function of temperature in foliar materials was much greater than that of the woody fuels, which were more linear in form. In a companion study to the present work, Amini et al. [23] used a thermogravimetric analyzer to derive kinetic parameters to model pyrolysis of foliar fuels. These kinetic parameters do not explicitly include heat capacity. Michaletz and Johnson [24] developed a model to predict crown scorch (foliage necrosis) from a wildland fire which assumed that the specific heat capacity of foliage was a mass-weighted average of dry biomass (apple) and the foliar moisture content. Clearly, water content is relevant, as Susott also noted, but an estimate for the specific heat capacity on a dry basis is still needed. A photothermal method was developed and applied to foliage to estimate heat capacity under ambient conditions [25]. While that study did not explore the temperature range used here, it provided a useful method for estimating C_p in a variety of leaves. An extensive review of the literature found limited information on the specific heat capacity of foliar fuels, particularly at temperatures associated with wildland fire. Our work aims to fill this gap by investigation of the foliar fuels studied by Weise et al. [1].

Given the limited C_p data on foliar fuels it is common to turn to wood and other biobased materials to gain insight into how C_p varies with temperature, but even those studies typically do not reach temperatures over 300 °C. For example, the Wood Handbook [26] provides a simple linear increase in wood C_p with temperature up to 147 °C, while Dupont et al. [27] also provide a linear correlation for wood and other biomass up to 80 °C. Further, they study char to higher temperatures but note the presence of "exothermal phenomenon" which occur in char at these higher temperatures. A recent study of C_p in common building materials, including wood, also limited the investigation to under 300 °C [28]. Our aim in this investigation was not only to focus on foliar fuels but also to explore temperatures up to 434 °C, the highest temperature for which we could get reliable data without damaging our DSC.

1.2. Complexities in determination of specific heat capacity

The interaction of several physical mechanisms occurring between 180 and 500 °C and the range in thermal characteristics of the components of foliar fuels complicates the measurement of heat capacity. Simplified expressions of heat capacity typically refer to a material that is assumed to not change in structure and function with time. Thybring [29] explores the underlying mechanism of molecular vibration and rotation in cellulose, hemicelluloses, and lignin to provide physical insight into the increase of C_p with temperature. However, for live vegetation temperatures above 180 °C, physical mechanisms associated with pyrolysis produce a more complex relationship between heat capacity and temperature as seen by Susott [3]. Hereafter, the heat flows from these additional mechanisms will be referred to as 'heats of reaction' following Cho et al. [30]. Heats of reaction can be either exothermic or endothermic depending on the kinetics of the chemistry and the physical setting (heating method, sample holder, and other details which can influence secondary pyrolysis). The onset of processes that contribute to heats of reaction occur at the onset of mass loss as chemical components enter the gas phase and leave the calorimeter. Werner et al. [31] described a suite of reactions, some of which may be occurring simultaneously, as "dehydration, depolymerization, fragmentation, rearrangement, repolymerization, condensation, and carbonization."

Table 1
Common woody plants from southern United States for which specific heat capacity was measured in triplicate.

Scientific name*	Common name	Label	Room MC (%)
Ilex glabra (L.) A. Gray	inkberry	IB	3.9
Ilex vomitoria Aiton 'Schelling Dwarf'	yaupon	YH	4.2
Lyonia lucida (Lam.) K. Koch	fetterbush	FB	4.0
Morella cerifera (L.) Small	wax myrtle	WM	5.1
Persea palustris (Raf.) Sarg.	swamp bay	SB	4.0
Vaccinium arboreum Marshall	sparkleberry	Spark	3.7
Pinus palustris Mill.	longleaf pine	LLP	3.9
Quercus nigra L.	water oak	WO	5.1
Quercus virginiana Mill.	live oak	LO	4.6
Sabal minor (Jacq.) Pers.	dwarf palmetto	DP	4.3
Serenoa repens (W. Bartram) Small	saw palmetto	SP	4.1

* [34,35].

Cho et al. [30] and Werner et al. [31] illustrate some of the difficulties of using DSC for heat capacity measurement. Typically, in a DSC, a sample increases in temperature at a constate rate and variations in required energy input indicate phase transitions in the material. This is useful for investigation of heats of reaction, which was the focus for Cho et al. [30] and Werner et al. [31]. If there are not variations in the energy input that indicate a phase transition or heat of reaction, and the mass is constant, then the heat flow can be used to estimate C_p. However, when there are variations in heat flow, C_p must be assumed to study the heat of reaction. Inside a DSC cell, as a sample undergoes pyrolysis, energy flow is occurring for at least three reasons: (1) heat required to raise the temperature of the sample, C_p, (2) heat used to convert reactants into products, heat of reaction, and (3) heat lost to the surrounding environment via radiation and convection. For this study we used a complex pattern in the DSC temperature exposure to measure heat flow and thermogravimetric analysis (TGA) to measure mass loss during heating. Combined, these measurements allowed for the calculation of both the heat of reaction and C_p. As will be explored in more detail below (Section 2.3.1, Appendix A, and the results Section 3.2.2) the patterned energy input used in the DSC proves helpful for measurement of C_p during pyrolysis.

1.3. Objectives of this study

Both heat of combustion and C_p were briefly reported for the leaves of interest in previous work related to our larger project [32]. This paper provides details on the C_p measurements for these foliar fuels, with a focus on the DSC technique and results. We also shed light on the heats of reaction for the leaf species under investigation. A simple model was developed that fits the increase in C_p with temperature and is presented here. We then use this and the known composition of each of our leaves [33], to provide a method for estimation of the specific heat capacity of any leaf across a wide temperature range, assuming the leaf composition is known.

2. Materials and methods

2.1. Leaf species and preparation

Eleven plant species representing a range of potential wildland fuels in the southern United States were obtained from commercial nurseries and then grown indoors under grow lights allowing harvest of fresh plant leaves for specimens. Leaves were harvested, weighed, and then immediately dried in a vacuum oven at 45 °C to obtain moisture content (dry weight basis) and preserve chemical composition as close as possible to the live state. Mature leaves were sampled with minimal stem or stalk. Dried leaves were ground by Wiley mill to produce a uniform size powdered leaf material which fit through a 1 mm mesh (# 20) screen that was suitable for further chemical and thermal processing. The tested plant species are listed in Table 1. Ground powdered samples

were stored in a test tube inside a desiccator. However, while loading the specimens, they were exposed to lab conditions with a relative humidity (RH) between 40 and 50%. Because of this, samples quickly regained moisture to equilibrate with lab conditions. The resulting specimen moisture content (MC) is presented as 'room MC' in Table 1. Methods for estimation of the MC are described in the next section. For a control, Whatman #1 filter paper was used as a source of pure and mostly crystalline cellulose and processed similarly to the leaves. This material is described as cellulose (cell) in subsequent text and figures. Each 5–10 mg sample was placed in an aluminum capsule used by the calorimeter (DSC), or platinum cup for gravimetric analysis (TGA), described subsequently.

2.2. Determination of dry mass, mass loss, and mass loss rate

A Thermo Gravimetric Analyzer (PerkinElmer, Pyris 1 TGA) was used to measure mass loss during heating. The TGA was calibrated per the manufacturer's recommendation with the sample temperature accuracy of ± 2 °C. The TGA mass balance has resolution of 0.1 μg and accuracy of 0.02%. The primary output of TGA is mass, or mass fraction, versus temperature.

To determine the dry mass of the specimens, a 5-minute drying period at 105 °C was applied, which was more than adequate to ensure a dry sample (mass loss typically stopped near 2 min since the only moisture came from the room during transfer of the previously dried samples), and the dry mass taken at the end of this period. After the drying period, a temperature ramp rate of 3.5 °C/min was applied with nitrogen as the purge gas to prohibit combustion (flow rate 50 ml/min). The heating rate was chosen to match that needed for accurate C_p measurement as described in Section 2.3.1 and further below. Both the mass fraction and C_p, reported subsequently, were based on dry mass. The difference between the TGA starting mass and dry mass was used to compute the 'room MC' reported in Table 1. The mass fraction versus temperature data was also processed to yield a mass loss rate in units of % mass per minute. These plots are helpful for understanding the temperature at which various leaf components degrade. However, the primary interest in the present study was the mass fraction, calculated at 2 °C intervals, which was subsequently applied to the DSC sample mass to calculate C_p. The heating rate used in the present study was lower than the heating rates investigated by Amini et al. [23] in order to match the slower DSC heating rate which allows a more accurate determination of specific heat capacity because the sample can more easily match the applied temperature.

2.3. Determination of specific heat capacity and heat of reaction

2.3.1. Introduction

The C_p for each leaf was measured with a differential scanning calorimeter (DSC) (TA Instruments, DSC Q2000)[2]. We used the manufacturer-provided modulated DSC® method [36] which adds a sinusoid-patterned energy to a linear temperature ramp. The patterned energy input was used to calculate C_p based on the amplitude of the sinusoidal energy input and the resulting sinusoidal temperature change. Focus on the smaller heat flows associated with the sinusoidal variation provide a more accurate measurement of C_p. Using this method, the effects of energy transfer to the environment and heat of reaction are reduced. Further details and history on this method are provided by Danley [37]. All samples were processed with the same 3.5 °C/min linear ramp and a modulation period of 100 s with amplitude of 0.93 °C. These slow changes allow the sample to track the applied temperature pattern. The initial specimen mass was recorded and assumed to be at 'room MC', so the dry mass was calculated from the mass at 'room MC'.

Using the patterned energy input with the linear temperature ramp rate allows calculation of two heat capacities: C_p and the total specific heat, C_{total}. While the C_p measurement screens out most of the heat of reaction effects, the total specific heat capacity C_{total} considers all of the energy needed to maintain the temperature rise. This total heat flow is automatically measured and calibrated by the instrument just like C_p. The total C_{total} is comparable to Susott's method which can identify the effects of heat of reaction during pyrolysis (from chemical reaction or phase change). Calculating both C_p and C_{total} allows an estimation of the effective heat of reaction by subtracting C_p from C_{total}.

2.3.2. Calibration

Calibration for the specific heat measurements took place in two stages. The first stage was a basic calibration to determine the instrument energy input and temperature measurement. The second stage refined the C_p measurement. All calibration stages relied on sapphire disks of known mass. In the first stage, the sapphire disks were placed directly on the thermopile stand allowing calibration of the energy input. The first calibration stage was completed with a specimen of indium in a sample holder. Indium's well-known melting temperature and heat of fusion determine the temperature calibration of the thermopiles. This first stage in calibration followed the manufacturer's recommendations to provide a temperature accuracy of ± 0.1 °C and a calorimetric reproducibility (from the indium heat of fusion) of ± 1%. In the second stage of the calibration, with focus on the specific heat capacity, sapphire disks inside an aluminum capsule sample holder were placed on the thermopile. A correction factor, based on the known C_p for sapphire, was calculated and applied so that the instrument reported specific heat capacity was modified to yield a more accurate C_p. Details on this method, which went beyond that recommended by the manufacturer, are provided in Appendix A, which includes a discussion of the total measurement uncertainty which was 4% before the onset of pyrolysis.

2.3.3. Operating conditions

The DSC maintained a pure nitrogen environment around two capsules, one of which had no sample and was used to subtract out the effect of the aluminum sample holder while the other capsule held the specimen. The sample size ranged from 4 to 14 mg depending on the leaf species in a sample holder of mass near 51 mg. Each capsule sat on a thermopile allowing precise temperature measurement while being heated from below with a precisely measured energy input. The temperature ramp rate was 3.5 °C/min, similar to the ramp rate applied in the TGA. However, the maximum temperature was limited to 434 °C and the drying period before C_p measurement was extended to 30 min at 120 °C to ensure the sample inside the aluminum holder had dried out (the sample lid slows moisture loss). After the initial drying period, the temperature was reduced to −20 °C before beginning the temperature ramp up to 434 °C.

2.3.4. Data analysis methods

Each leaf species in Table 1 was measured three times and the average is reported. The results section provides an example of the sample variability by plotting the 95% confidence interval based on the measurements of the 3 different samples of the same species. Data analysis continued by fitting each individual leaf species to its own power function which captures the linear rise in C_p with temperature until it stops rising at T_{max}. After T_{max} the specific heat capacity is modeled as a constant C_{max}. Thus, the C_p data for each species was fit to a simple power function as in Eq. (2).

$$C_p = C_{max}[T/T_{max}]^n \text{ while } T < T_{max} \quad (2)$$

T and T_{max} are temperatures in Kelvin. C_{max} is a fit parameter which is the maximum specific heat which occurs when the temperature

[2] The use of trade or firm names in this paper is for reader information and does not constitute endorsement by the U.S. Department of Agriculture of any product or service.

Table 2
Leaf composition, percentage by dry mass of select components.

Common name	Lipid	Sugar	Prot[3]	Pect	HC	Cell	Starch	Phen	Lig	Min	Sili
yaupon	31.3	3.7	8.7	1.9	7.3	8.8	0.0	6.6	25.2	4.5	0.4
fetterbush	30.0	4.0	4.9	1.8	6.9	16.6	0.0	3.4	30.3	2.2	0.3
inkberry	28.1	4.2	5.3	2.6	5.4	11.1	2.2	9.0	25.0	1.9	0.0
longleaf pine	22.3	2.3	7.4	2.0	15.0	19.0	0.7	3.1	23.5	2.0	0.6
wax myrtle	15.6	1.7	14.1	2.7	10.5	17.6	0.3	2.4	28.1	2.5	0.2
water oak	15.1	2.9	8.8	2.9	5.8	15.7	0.9	13.5	25.3	3.1	4.3
saw palmetto	11.9	1.3	5.4	0.7	18.6	11.0	1.0	4.8	29.8	1.8	4.8
swamp bay	11.3	4.1	8.3	1.8	10.5	18.3	0.8	5.3	32.9	1.9	0.0
live oak	9.9	2.6	14.0	1.7	10.9	19.2	0.7	5.8	23.7	2.9	0.0
dwarf palmetto	6.8	2.3	12.9	2.0	18.0	28.0	0.6	7.9	17.1	3.3	1.1

[3]To include all twelve components, the following abbreviations were used: Prot = proteins; Pect = Pectin; HC = hemicellulose; Cell = cellulose; Phen = phenols; Lig = lignin; Min = minerals; Sili = silicates.

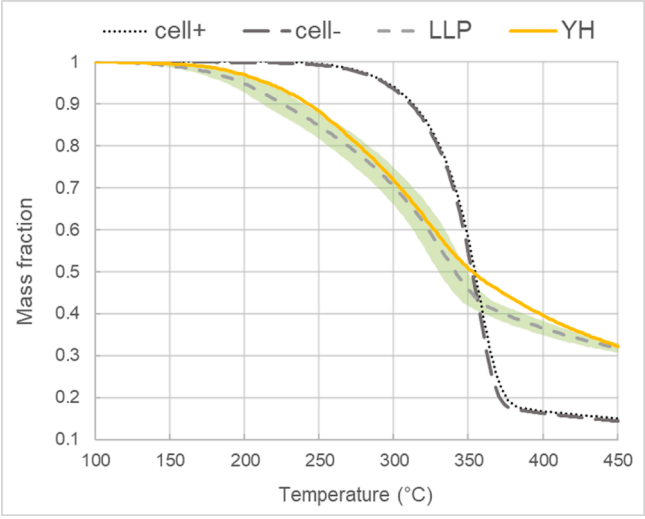

Fig. 1. Fraction of dry mass versus temperature during pyrolysis for cellulose (cell, from Whatman paper), LLP, and YH.

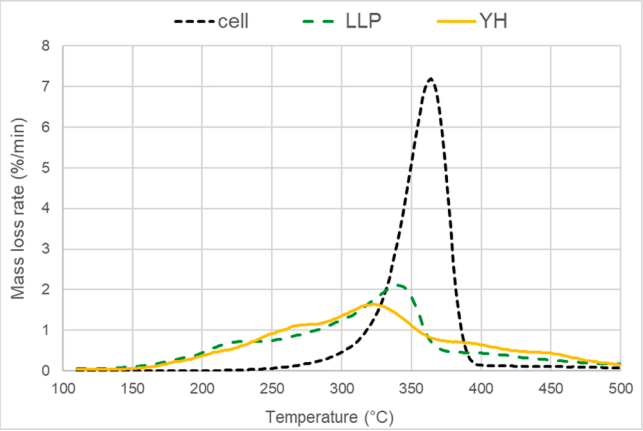

Fig. 2. DTG curves (mass loss rate versus temperature from TGA data) for example samples of cellulose, LLP, and YH.

exceeds that of T_{max}, which is another fit parameter. The final fit parameter, n, is the power to which the temperature ratio is raised. This model captures the basic shape of a steady rise until T_{max} after which C_p is constant.

Next, a more general approach to fitting the data is presented which used information about the leaf composition [33] rather than the individual species, but again takes the power function form of Eq. (2). In this method, each leaf component (lipids, cellulose, etc.) was modeled as a power function. The final composite n, T_{max}, and C_{max} for each plant species were mass averages of each component based on the composition. A brief summary of the composition analysis work is outlined below.

2.4. Leaf composition

Using the leaf composition results of Matt et al. [33], a leaf heat capacity estimation method was developed. Ten of the leaf species (excluding sparkleberry) were analyzed into twelve chemical groups: lipids, nonstructural sugars (glucose, fructose), protein, pectin, hemicellulose, cellulose, starch, phenol, structural lignin, minerals, and silicates. Table 2 provides the percentage of components based on dry mass, sorted by percentage of lipids.

For this table the two sugars were combined. However, each individual component was used in the heat capacity estimation method which relies on an estimate of C_p for each component. The total leaf C_p is then a mass weighted average of the leaf components, each component of which is modeled using Eq. (2). Of course, using a composition analysis to calculate C_p will always be less accurate than direct measurement. The composition analysis itself introduces uncertainty. The methods used by Matt et al. [33] typically accounted for 95 to 100% of all sample mass and they provide further details on individual component uncertainty in the paper.

3. Results

3.1. Mass and mass loss rate

The results for mass fraction versus temperature for selected samples are provided in Fig. 1. Four TGA runs were conducted using cellulose from Whatman paper (cell), one run for yaupon (YH), and two runs for long leaf pine (LLP). The fractional mass was computed every 2 °C. The cellulose output is plotted as black lines showing the upper and lower bound of the 95% confidence interval (cell+, cell−) primarily to demonstrate the repeatability of the TGA data. The two runs of LLP illustrate greater variability in the leaf materials by plotting the average value (dashed line) and 80% confidence interval as light shading. However, since the mass was not directly measured during the determination of C_p, this variation was not explored further in this paper. Instead, the mass fraction determined by TGA for each leaf species was applied to the corresponding C_p measurements. The YH data is included in Fig. 1 as it is the example species in all the results to follow. The results for single runs of all species are provided in Appendix B.

The cellulose mass fraction decreased sharply compared to the leaves, which contain multiple components including cellulose that pyrolyze at different temperatures. For the same reason, the leaves started losing mass at lower temperatures relative to the cellulose. The remaining mass at temperatures above 400 °C was much higher in the

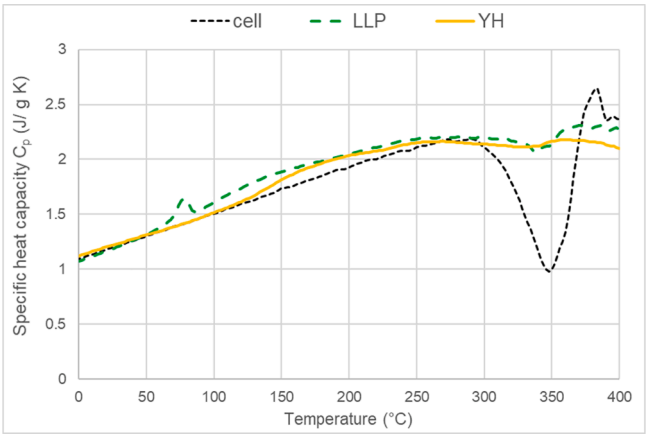

Fig. 3. Specific heat capacity versus temperature during pyrolysis for cellulose, LLP, and YH.

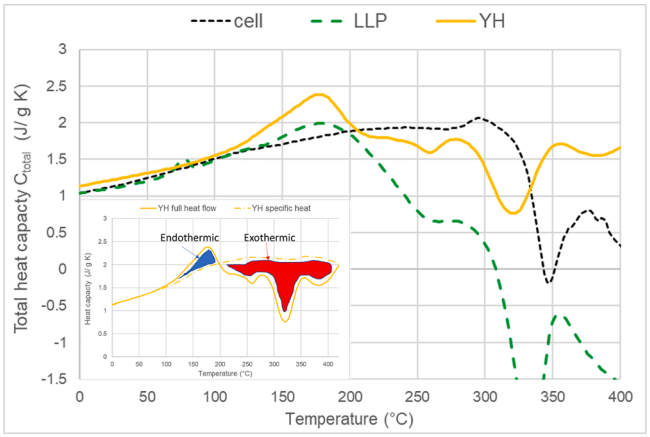

Fig. 4. Total specific heat capacity, C_{total}, versus temperature during pyrolysis for cellulose, LLP, and YH. Lower left insert plots both total and specific heat capacity for YH and illustrates the endothermic and exothermic temperature regions.

leaves (compared to cellulose) because some components of the leaves had not yet fully degraded, as seen in the mass loss rate curves of Fig. 2.

Fig. 2 plots the differential thermogravimetric curve (DTG), which is the mass loss rate versus temperature for the same specimens presented in Fig. 1. The units for mass loss rate are in % mass per minute, from the same mass fraction data but multiplied by 100 to get 100% mass at start (after initial dry out). The DTG curves highlight any change in rate of mass loss with peaks that represent active pyrolysis of the material and troughs between the peaks that represent overlapping reactions. Simpler materials have a rapid degradation with a single peak, while more complex materials can have multiple peaks and the degradation is spread across a larger temperature range. This is evident in Fig. 2 with the single peak for cellulose occurring between 250 and 390 °C while the leaf material had peaks occurring over a larger temperature range between 150 and 450 °C. This pyrolysis temperature range for cellulose corresponds with literature values, which depend somewhat on the heating rate [38,39]. The larger temperature range present for the leaf materials improves the measurement of C_p when using the patterned energy input.

Mass loss rate plots for all species are provided later (see Section 3.6, Fig. 10).

3.2. Heat capacity

3.2.1. Initial examples and discussion

The C_p results for selected samples are plotted versus temperature in Fig. 3. Plots for all species are in the next Section 3.2.2. All DSC results were averages with the DSC calibrated as already described (Section 2.3.2).

Inspection of Fig. 3 reveals that the leaves are similar to pure cellulose (cell, from the Whatman paper) in their general rise in C_p with temperature. However, we note the brief bump up in C_p for the LLP between 50 and 100 °C, which most likely reflects an endothermic heat of fusion from melting of a component(s) from LLP at low temperatures. Similarly, the cellulose (cell) data show a larger deviation from the gentle rise around the temperature where the cellulose is undergoing rapid mass loss, indicating an exothermic heat of reaction. Our method for determination of C_p works best when each component of the leaf has only a small value of energy release (heat of reaction) compared to the total heat flow, and these small component heat flows occur over a wide temperature range to limit the effect of any one component heat of reaction on the C_p calculation at any particular temperature. This was the case with our leaves because they contain a variety of chemical components, each of which makes up only a fraction of the total mass and have different heats of reaction at different temperatures from each other. For all our leaf results, including Fig. 3, we report the average of three replicates. The variation recorded between replicates for C_p is illustrated below (see Fig. 7 in Section 3.4).

Using the patterned energy input with the linear temperature ramp rate allowed calculation of two heat capacities; C_p, which we just examined, and the total specific heat capacity, C_{total}, which takes into account all of the energy needed to maintain the temperature rise. Calculating the C_{total} is useful to compare our results with Susott [3] and it also allows an estimation of the effective heat of reaction by subtracting C_p from C_{total}. Fig. 4 plots C_{total} versus temperature for the same samples of cellulose, LLP, and YH just examined.

Measuring the full heat flow yields a much more complicated relationship of heat capacity to temperature. Both endothermic and exothermic heats of reaction can be inferred by comparing Figs. 3 and 4. An example of the endothermic and exothermic regions for YH is provided in the Fig. 4 lower left insert. Thus, for example, both the YH and LPP have a faster increase in C_{total} (compared to cellulose) near 175 °C, which indicates an endothermic reaction is occurring, requiring more heat input to allow the temperature to rise. But this is short-lived and exothermic reactions dominate at higher temperatures, with the LLP showing very strong heat release during pyrolysis (between 300 and 350 °C). At temperatures over 400 °C pyrolysis is almost over and C_{total} returns toward its original values. These effects will be explored in more detail in Section 3.6. Figs. 3 and 4 were included to illustrate the differences between C_p and C_{total} that can be measured with this instrument using the patterned energy input.

3.2.2. Overview of C_{total} and C_p for all leaves

Fig. 5 plots both C_{total} and C_p for all 11 species in one figure for easy comparison.

The total heat capacity (C_{total}, left of Fig. 5) clearly shows the heat of reaction that occurs at temperatures over 180 °C when C_{total} stops its gentle rise with temperature. All leaves have an exothermic heat of reaction just above 300 °C, with longleaf pine (LLP) showing the strongest reaction given a negative C_{total}. However, C_p (right of Fig. 5) shows a gentle rise with temperature until near 200 °C when it begins to level out. Each leaf also has a slight dip in C_p above 300 which may be an artifact from the high heat of reaction we see in C_{total}, which could not be completely filtered out when using the sinusoidal signal processing to calculate C_p. The heats of reaction will be examined in more detail below (Section 3.6)

3.3. Comparison to Susott data

A comparison of our YH and LPP data with the only live fuel Susott

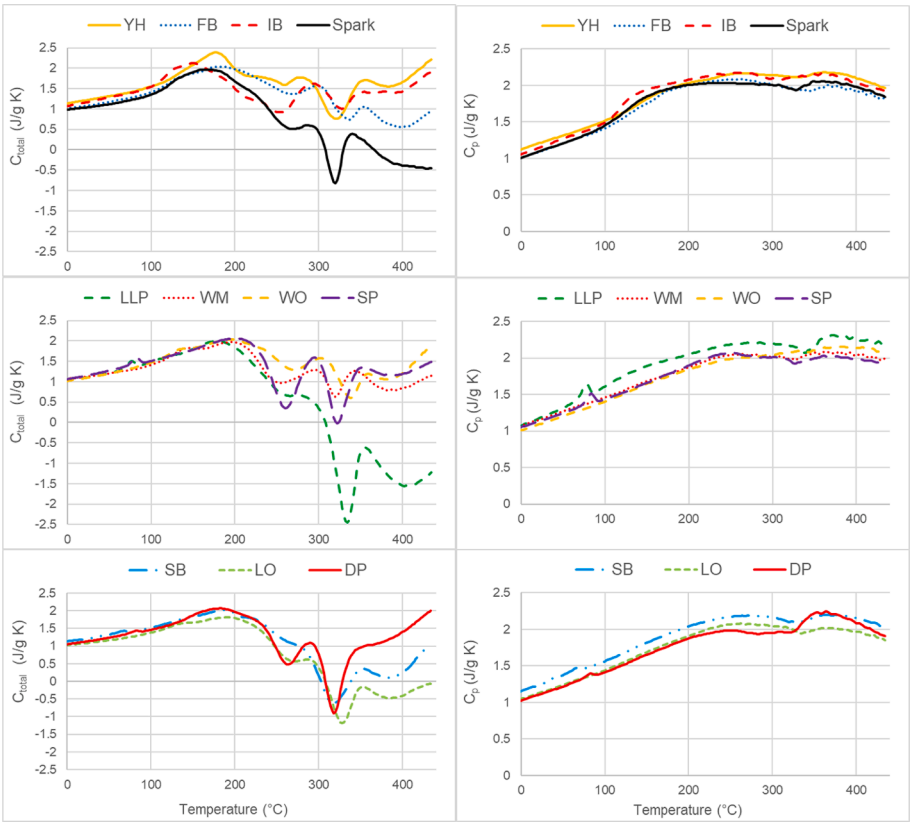

Fig. 5. C_{total} (left) and C_p (right) for all leaf species.

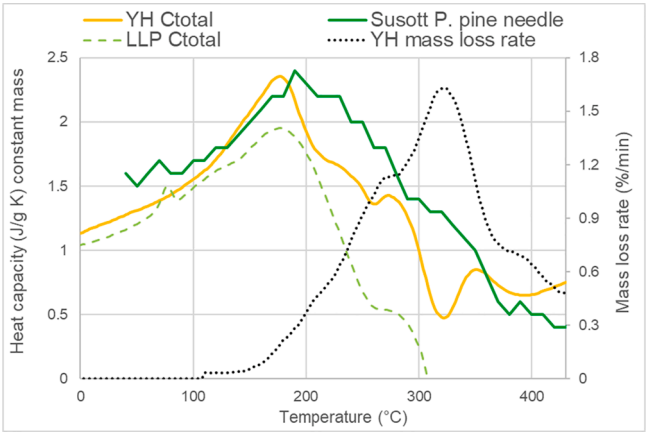

Fig. 6. Susott live fuel total heat capacity on constant mass basis data compared to YH and LLP, with YH mass loss rate (%/min) on right y-axis.

[3] studied, green ponderosa pine needles, is provided in Fig. 6. In order to facilitate the comparison, C_{total} is plotted on a constant mass basis using the initial mass. Since the mass adjustment was not utilized, the heat capacity curves in Fig. 6 appear different from Fig. 5. Both Susott's pine and our YH and LLP C_{total} measurements show a similar initial shape with the peaks occurring in similar temperature ranges. All C_{total} measurements then decline after 200 °C.

However, the YH had a more significant exothermic heat release between 200 and 350 °C than the Susott pine, and the LLP is even more extreme. Note that this exothermic reaction in YH C_{total} corresponds to the strong increase in mass loss rate near 320 °C. The heat release profile corresponds to the mass loss profile (shown as the dotted black line with right axis y-scale), which is usually associated with charring of the

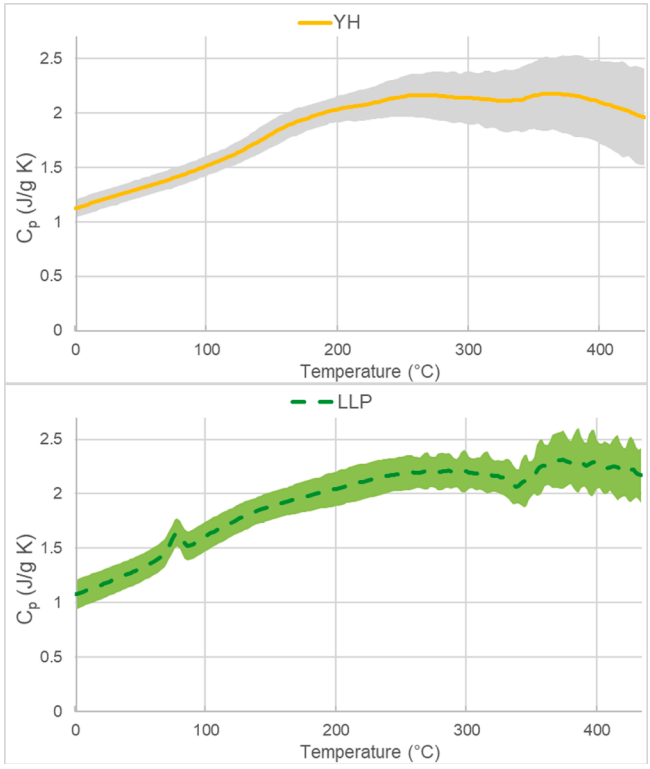

Fig. 7. Mean Cp of YH (top) and LLP (bottom) with 95% confidence interval shaded.

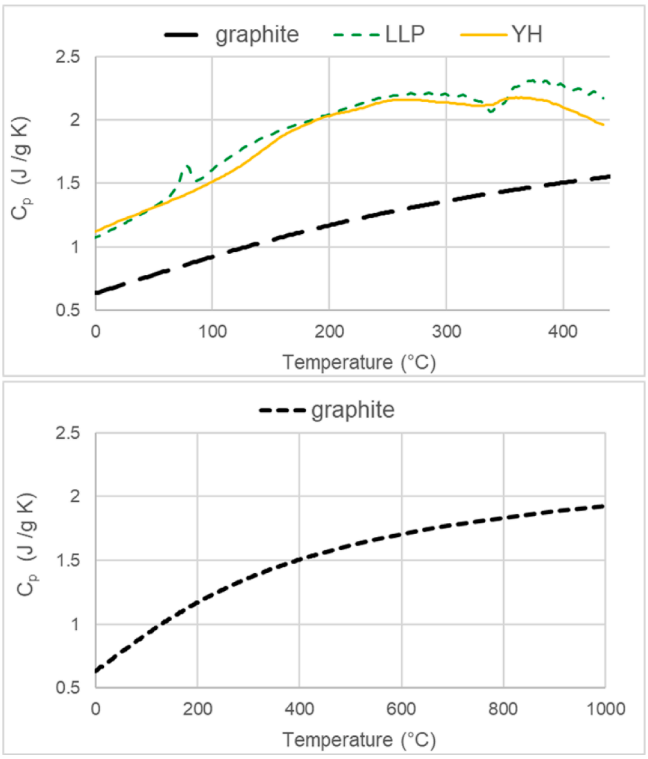

Fig. 8. Select leaf C_p compared with graphite (top) and graphite C_p to higher temperature (bottom).

lignin, hemicellulose, and cellulose [30]. While not all leaf species tested had such large drops in C_{total}, all species undergo exothermic reactions in this temperature range.

3.4. Basic trends in C_p and comparison to graphite

The overall trend for all 11 species showed an increase in C_p with temperature until peaking between 175 and 275 °C after which they are generally flat (Fig. 5). This increase in C_p with rising temperature (until the onset of pyrolysis) is widely reported in biomass materials [27]. Dupont et al. [27] model the C_p rise with temperature as linear between 40 and 80 °C. To illustrate the variability of results during a DSC run Fig. 7 plots the average value (line) and 95% confidence interval as light shading for both YH (top) and LLP (bottom) based on the 3 replicates. This confidence interval does not include the uncertainty in the C_p measurement as a result of all sources of potential error, but only the uncertainty based on the standard deviation from the calculated result of three different runs, much of which is due to inherent sample variability. The other influences on the accuracy of the final result are discussed in Appendix A.

Comparing these results with those for graphite provides insight into the carbon-dominated form of the leaf material after pyrolysis. Graphite, using data from Butland & Addison [40], is plotted along with longleaf pine and yaupon in Fig. 8(top). Fig. 8(bottom) expands the graphite data to higher temperatures. The pure graphite C_p levels out near 1000 °C but not as quickly as the leaf samples. We speculate that the charring process slowly turns leaf components into a carbon form that mimics graphite in its behavior of C_p with temperature. However, it is likely that char chemical structure contains very little of the crystalline carbon which characterizes graphite. The chemical structure of char varies by temperature and the process of formation [41].

3.5. Modeling results

For modeling, a simplified formula to characterize the variation of C_p with temperature would be useful. Review of the graphite (Fig. 8) and Whatman paper (Fig. 3) data shows the same C_p increase at low temperatures. This behavior was also observed in our foliar materials (Fig. 5, right). A power function fit captures this increase, although it is also commonly modeled using a linear slope and offset [27]. Both functional types can fit the biomass C_p rise for temperatures under 200 °C. However, the leaf C_p stops increasing at higher temperatures so the power function must be scaled to a maximum temperature after which C_p can be treated as constant. In the next sections we present results based on this mathematical form described in Eq. (2) in methods Section 2.3. Then we show how this approximation can be extended to a composition based fit useful for biological materials for which C_p has not been measured but is needed for modeling.

3.5.1. Individual species fit

The C_p data for each individual species was fit to the simple power function of Eq. (2). Examples of individual leaf fits are plotted in Fig. 9, while the fit values for n, C_{max}, and T_{max} for each leaf species are presented in Table 3. The material composition was changing after T_{max} due to pyrolysis, but C_p is nearly constant for all our leaf species.

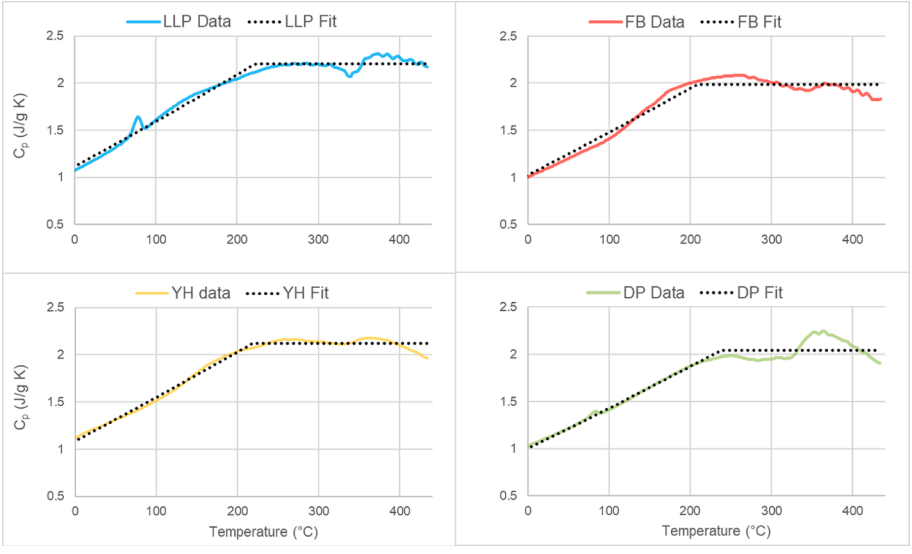

Fig. 9. Specific heat for select leaves with fits to Eq. (2): LLP, FB, YH, DP.

Table 3
Summary of parameter estimates and fit statistics for power function for specific heat of individual species.

Label	Common name	n	Cmax	Tmax (K)	Tmax (°C)	RMSE	Err (% Cmax)	% StdDev
FB	fetterbush	1.162	1.99	481	208	0.063	3.2%	10.9%
DP	dwarf palmetto	1.135	2.04	511	238	0.072	3.5%	3.4%
LLP	longleaf pine	1.140	2.20	496	223	0.052	2.4%	4.3%
LO	live oak	1.138	2.05	504	231	0.013	0.6%	4.2%
SB	swamp bay	1.127	2.15	491	217	0.034	1.6%	3.0%
IB	inkberry	1.164	2.10	478	205	0.068	3.2%	6.6%
SP	saw palmetto	1.133	2.00	494	221	0.033	1.7%	4.0%
WO	water oak	1.133	2.08	528	255	0.037	1.8%	5.6%
YH	yaupon	1.140	2.12	492	219	0.039	1.8%	4.9%
WM	wax myrtle	1.126	2.03	501	228	0.027	1.3%	6.3%
Spark	sparkleberry	1.164	2.02	479	206	0.047	2.3%	8.8%

Table 4
Leaf components and associated C_{max} for the composition model (n = 1.14, T_{max} = 497 K, fixed).

Leaf component	C_{max}
Lipids	2.22
Glucose	2.0
Fructose	2.0
Protein	2.0
Pectin	1.9
HemiCell	1.9
Cellulose	2.1
Starch	2.1
Phenol	2.2
Lignin	2.2
Mineral	1.1
Silicate	1.1

Goodness of fit was determined by the root-mean-square-error (RMSE) between data and fit. The overall RMSE was 0.047 J/g K. If all the data is fit with only one curve, ignoring the individual species, the overall RMSE nearly doubles to 0.081 J/g K, with n = 1.14, T_{max} = 497 K, and C_{max} = 2.08 J/g K.

The values for n in Table 3 are slightly above unity, which is consistent with the linearity shown in Fig. 3 for temperatures less than 100 °C. The values for C_{max} of the leaf species are similar to C_{max} for graphite at 1000 °C. Table 3 also includes a column (Err) which illustrates the model error (% of RMSE compared to C_{max}). This can usefully be compared to the average standard deviation from individual sample variation for each species (% StdDev) and the overall accuracy of the measurement (4%). Inspection of Table 3 shows that the model error is less than the measurement accuracy, and the sample variation itself is often greater than the measurement accuracy. The C_p and associated standard deviations at 2 °C intervals are provided across the full temperature range for each leaf species in the supplemental material in Appendix C.

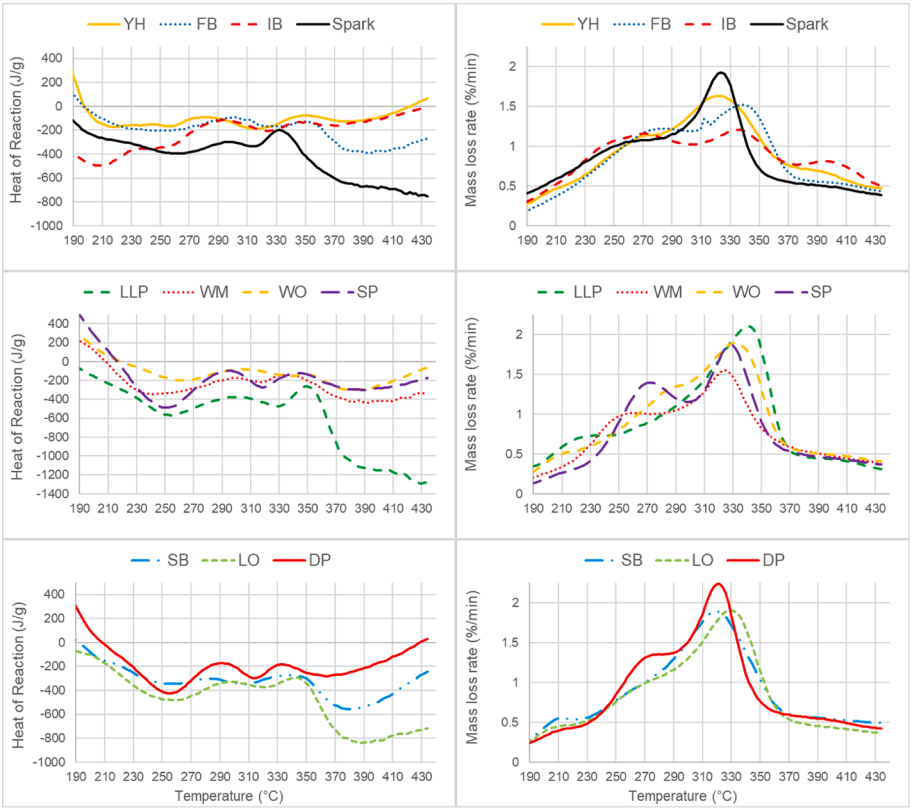

Fig. 10. Effective Heat of Reaction for all leaf species (left) and associated mass loss rate (right).

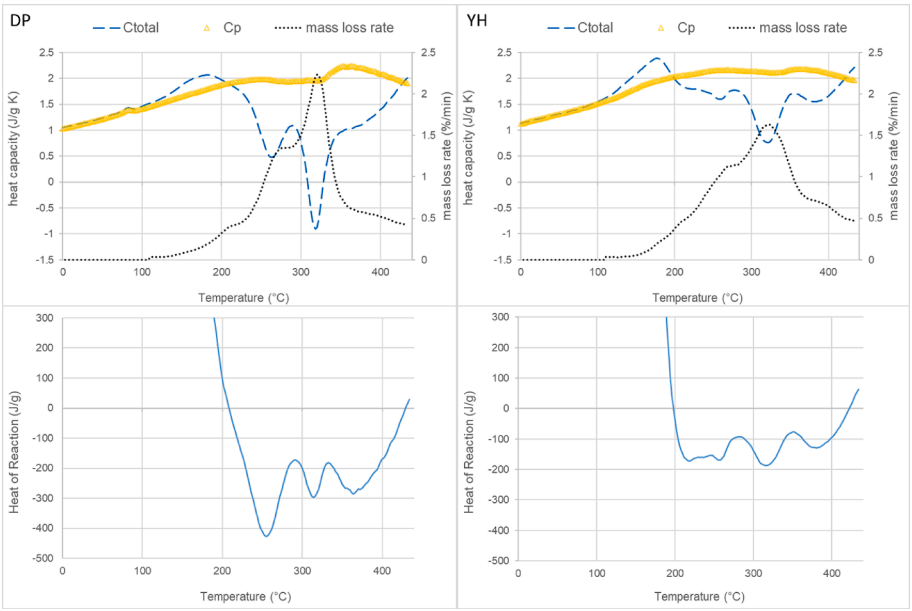

Fig. 11. Heat capacities of dwarf palmetto (DP, left) and yaupon (YH, right) with associated heats of reaction (bottom).

3.5.2. *Composition model fit*

Recall that in the composition model fit, each leaf component (lipids, cellulose, etc.), rather than the individual species, was modeled as a power function from Eq. (2). This fit succeeds because the components have a linear profile of C_p versus temperature (for temperatures less than 100 °C) as seen for the components plotted in Figure A-2. Both $n = 1.14$ and $T_{max} = 497$ K were fixed for the compositional model because their variation by component did not significantly improve the fit. The components and their associated C_{max} values are in Table 4. The overall RMSE was 0.074 J/g K, slightly better than just fitting all the data, but not as good as the individual species fit. The compositional fit can be improved, reducing the RMSE to near that of the fit by individual species, by allowing C_{max} of the lipids to vary by species. This compositional model provides a way to estimate C_p for any foliar material over the full temperature range of pyrolysis given the composition and may be adequate for use in fire models. It could be refined by testing additional leaves and a more detailed investigation of C_p for leaf components, with special attention to the variability in lipids.

3.6. *Effective heat of reaction and discussion*

An effective heat of reaction (energy change per mass undergoing reaction) can be calculated using C_p and C_{total} along with the mass loss rate ($\dot{m}$) from the TGA. The heat of reaction (ΔH) was calculated as in Eq. (3).

$$\Delta H = \left(C_{total} - C_p\right) m_{fraction} \left(m_0/\dot{m}\right) \dot{T} \tag{3}$$

where $m_{fraction}$ is the mass fraction of the original mass (m/m_0) at the temperature where the specific heat was measured, and $\dot{m}$ is the associated mass loss rate (mg/min) given the original dry mass, m_0 (mg), and $\dot{T}$ is the temperature change rate (heating rate) which was 3.5 °C/min.

The resulting heat of reaction and associated mass loss rates are plotted for all species in Fig. 10.

At low temperatures, below 200 °C, the effective heat of reaction may be endothermic, but at higher temperatures all the leaf samples show exothermic behavior, even under pure nitrogen. The exothermic heat region has a broad peak from 220 to 350 °C which allows it to be effectively screened out when using the sinusoidal technique to find C_p. Apparently, C_p is not particularly sensitive to the degradation process, thus simplifying its use in physics-based fire models.

Table 5
Heat of reaction for all leaf species.

Label	Common name	Heat of reaction (J/g)
FB	fetterbush	−190
DP	dwarf palmetto	−230
LLP	longleaf pine	−490
LO	live oak	−420
SB	swamp bay	−330
IB	inkberry	−210
SP	saw palmetto	−220
WO	water oak	−130
YH	yaupon	−120
WM	wax myrtle	−250
Spark	sparkleberry	−380

The influence of heat of reaction can be further illustrated by close inspection of Fig. 11.

The complex mixture of component reactions occurring above 200 °C often produces a small and nearly stable exothermic net effect between 220 and 350 °C. Tang and Eickner [42] and later Nassar and MacKay [43] both showed that charred lignin can produce a strong heat release. Similarly, Faleeva et al. [44] reported that hemicellulose also gives off heat during thermal decomposition. Yang et al. [45] also measured exothermic heat flow during pyrolysis of both hemicellulose and lignin. These and other components in the leaf will contribute to the different mass loss rate peaks with the corresponding peaks in the exothermic heat release rate that are apparent in Fig. 11. With detailed pyrolysis models and component thermophysical properties it may be possible to predict these net effects. The range of net heat of reaction is displayed in Table 5 which provides the average net heat of reaction (average weighted by mass loss rate) for all leaf species studied. These values can be compared to the heat of reaction for hemicellulose which is in the range of negative 100–500 J/g depending on the compound and how it chars [46]. For example, Werner et al. [31] report a value near −400 J/g for Xylan. Negative values indicate an exothermic reaction.

4. Conclusion

The specific heat capacity, C_p, of a range of leaf species was measured across a wide temperature range up to 434 °C. Despite complex effects of pyrolysis that begin near 180 °C, C_p for the partially pyrolyzed leaves

tends to be stable at temperatures above 200 °C. A simple power function was presented for future modeling efforts that fits C_p over this wide temperature range. Further, we provide a method to estimate C_p for a variety of plant species if their composition is known. Finally, data on the total heat capacity, C_{total}, was reported which supports examination of the complex pyrolysis effects, including the effective heat of reaction. The effective heat of reaction for all leaf species was reported, with speculation about lignin charring and hemicellulose heat of reaction as possible reasons for the exothermic heat release seen at temperatures above 220 °C.

CRediT authorship contribution statement

Charles R. Boardman: Methodology, Software, Validation, Formal analysis, Investigation, Data curation, Writing - original draft, Writing - review & editing, Visualization. **Mark A. Dietenberger:** Methodology, Formal analysis, Resources, Writing - review & editing, Visualization, Supervision. **David R. Weise:** Conceptualization, Resources, Writing - original draft, Writing - review & editing, Visualization, Project administration, Funding acquisition.

Declaration of Competing Interest

The authors declare that they have no known competing financial interests or personal relationships that could have appeared to influence the work reported in this paper.

Acknowledgements

This research was funded by DOD/EPA/DOE Strategic Environmental Research and Development Program Project RC-2640, funded thorough Contract 16-JV-11272167-024, administered by the USDA Forest Service PSW Research Station. We are grateful for help from a number of Forest Product Laboratory colleagues. Kara Yedinak and Laura Hasburgh both provided very helpful feedback and editing suggestions which improved the paper focus and presentation. Philip Walsh provided access and support in use of the TGA. Fred Matt provided support in sample preparation.

Appendix A

Details on the heat capacity correction factors and total error

Measurement of an accurate C_p in a differential scanning calorimeter requires extra care. In addition to the first stage of calibration, C_p measurement requires adjustment of the C_p reported by the instrument due to variations in the heat transfer occurring between the samples and the surrounding environment. This environmental heat transfer was found to depend on the temperature of the samples. The standard procedure recommended by the manufacturer is to define a single calibration factor, good for a narrow temperature range, which is used to adjust the instrument reported value. That calibration factor is calculated based on a sapphire sample in a holder subjected to the patterned temperature rise used for all specific heat capacity measurements. The heat capacity of sapphire is well known across a large temperature range.

This calibration factor varies by base temperature, temperature rise rate, and details of the sinusoidal signal. Since the single factor is good for only a narrow temperature range, the manufacturer recommended procedure would have yielded unacceptably large errors across the large temperature range desired for this study. Instead, we used a full calibration curve to provide the required calibration factors across the full temperature range with a typical error of ±4%. A cubic spline fit of the uncorrected instrument C_p data was used to create calibration factors at 2 °C intervals. And, this procedure also works for the uncorrected C_{total} data, so another calibration curve was created for that uncorrected

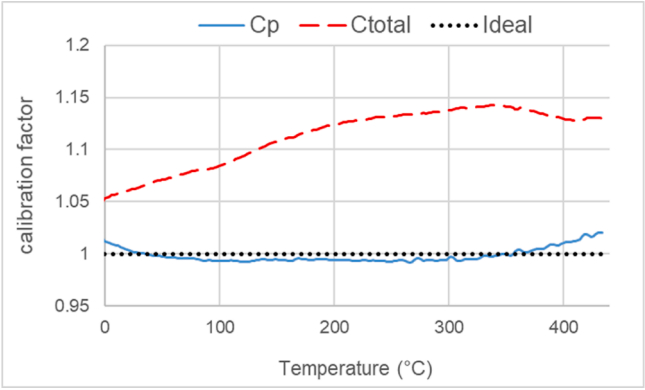

Fig. A1. DSC calibration factors for C_{total} and C_p.

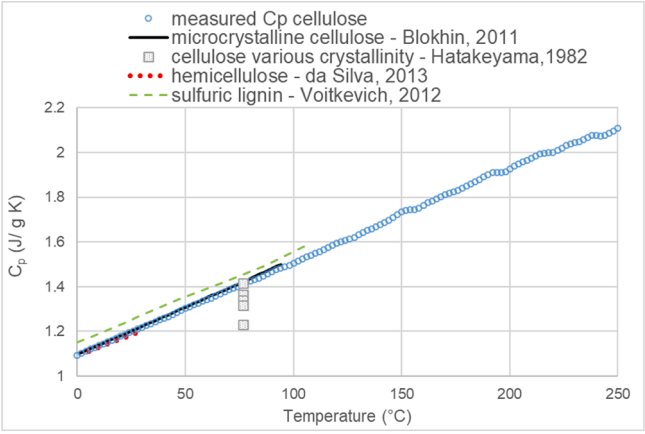

Fig. A2. C_p for various leaf components from literature values compared to measured Whatman paper cellulose.

instrument data. For sapphire, since there is no heat of reaction, C_p should equal C_{total} after applying the correction factors. Recall that C_p used the sinusoidal signal to calculate specific heat, while C_{total} used the base linear ramp rate. All of the measurements used a 3.5 °C/min ramp rate. We choose to add a sinusoidal period of 100 s, and sinusoidal temperature amplitude of 0.93 °C to this linear ramp based on manufacturer recommendations. To get a more accurate C_p the linear ramp should be slow and the sinusoidal period long, in order to allow the sample to follow the temperature curve.

Calibration curves for this instrument are plotted in Fig. A1. Each time the specific heat of a set of leaf samples was measured a sapphire sample was also included so that calibration curves specific to that set of runs were created and used to correct leaf data for both C_{total} and C_p.

In an ideal instrument, perfectly insulated from the surrounding environment, the calibration factor would be 1, shown as the ideal line in Fig. A1. The calibration curve for C_p is very close to 1, indicating that the slow sinusoidal calculation method works well. The calibration curve for C_{total} ,which has a larger deviation from ideal, gives some indication of the heat lost to the environment in the DSC cell.

Comparison of cellulose specific heat with literature values

To further check the calibration procedures the C_p of cellulose (from the Whatman paper) was compared to literature values. Fig. A2 plots the measured cellulose C_p along with selected literature values: Hatakeyama, Nakamura, & Hatakeyama [47] provide selected values at 77 °C for various types of cellulose which vary in crystallinity (heat capacity decreases with the increase in crystallinity), while Blokhin A.V. et al. [48] provide a range of values for microcrystalline cellulose which

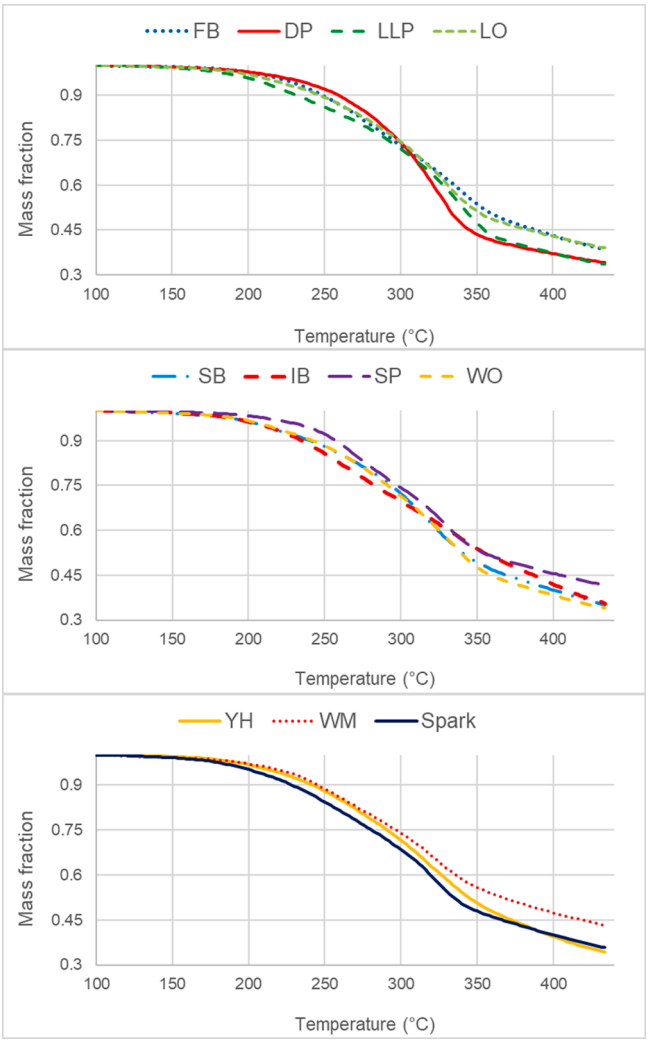

Fig. B1. Mass fraction versus temperature for all leaf species.

confirms the change in C_p with temperature at lower temperatures. Also plotted in Fig. A2 are results for other components in our leaf species, including an example hemicellulose from Ribeiro da Silva et al. [49] and an example lignin from Voitkevich et al. [50]. Inspection of Fig. A2 reveals our cellulose values best match those from the microcrystalline cellulose.

Discussion of total error in C_p, C_{total}, and heat of reaction

Uncertainty in the measurement of total heat flow typically makes the largest contribution to the uncertainty budget in a DSC [51]. This is true for our experiments only when the mass is well known. Under these conditions the calibration factor variation from run to run provides the best insight into overall accuracy and was estimated at 4% total error for the C_p measurement, primarily due to slight variations in lid placement from run to run which affects heat transfer to the environment. The uncertainty for C_{total} is similar when temperature is under 200 °C but rises to 10% error at 350 °C because of increasing loses to the environment which are not as well screened without the modulated method. The heat of reaction has even larger error bars because it is the difference between two separate measurements and is at least 15%. Other methods would be needed for more accurate heat of reaction measurements, which would still rely on a good estimate of C_p.

However, there are additional contributions to the absolute accuracy of C_p which arise from the changing mass once pyrolysis starts. The initial dry mass is known to better that 1%. Most of that initial mass error comes from the estimate of water content picked up while loading the sample. Once the sample starts losing mass the uncertainty increases, not because of the TGA mass loss curve itself, but because of the inherent variation in the sample behavior at high temperatures. The mass was not directly measured in the DSC, and the TGA curve approximates the actual mass loss for that particular run which is unknown. The effects of this potential mass loss mismatch appear as larger than desired variation between DSC runs. Further studies with combination TGA and DSC instruments could reduce this variation but were outside the scope of this study.

Appendix B

Plots of mass fraction versus temperature

While mass fraction was not the primary focus of this paper, Fig. B1 provides plots of mass fraction versus temperature for all leaf species because these data were used to calculate C_p.

Appendix C. Supplementary data

Supplementary data to this article can be found online at https://doi.org/10.1016/j.fuel.2021.120396.

References

[1] Weise DR, Fletcher TH, Johnson TJ, Hao W, Dietenberger M, Princevac M, et al. A project to measure and model pyrolysis to improve prediction of prescribed fire behavior. In: Viegas, D X, Ed Advances in Forest Fire Research 2018 Coimbra, Portugal: Imprensa Da Universidade de Coimbra p 308-318 2018:308–18. doi: 10.14195/978-989-26-16-506_33.

[2] Hough WA. Caloric Value of Some Forest Fuels of the Southern United States. Res Note SE-120 Asheville, NC: US Department of Agriculture, Forest Service, Southeastern Forest Experiment Station 6 p 1969;120.

[3] Susott RA. Differential scanning calorimetry of forest fuels. For Sci 1982;28: 839–51. https://doi.org/10.1093/forestscience/28.4.839.

[4] Rothermel RC. A mathematical model for predicting fire spread in wildland fuels. Res Pap INT-115 Ogden, UT: US Department of Agriculture, Intermountain Forest and Range Experiment Station 40 p 1972;115.

[5] Graves HS. Protection of forests from fires. Washington, D.C., USA: USDA Forest Service; 1910.

[6] Fons WL. Analysis of Fire Spread in Light Forest Fuels. Journal of Agricultural Research 72 (3): 92-121 1946;72:92–121.

[7] Byram GM, Fons WL. Thermal properties of forest fuels. Interim Technical Report AFSWP - 404 Division of Fire Research, Forest Service, US Department of Agriculture 34 p 1952.

[8] Byram GM, Fons WL. Thermal conductivity of some common forest fuels. Interim Technical Report AFSWP - 405 Division of Fire Research, Forest Service, US Department of Agriculture 14 p 1952.

[9] Countryman CM, Philpot CW. Physical characteristics of chamise as a wildland fuel. Res Paper PSW-RP-66 Berkeley, CA: Pacific Southwest Forest & Range Experiment Station, Forest Service, US Department of Agriculture; 16 p 1970;066.

[10] Susott RA, DeGroot WF, Shafizadeh F. Heat content of natural fuels. J Fire Flammabil 1975;6:311–25.

[11] White RH, Zipperer WC. Testing and classification of individual plants for fire behaviour: plant selection for the wildland–urban interface. Int J Wildland Fire 2010;19:213–27. https://doi.org/10.1071/WF07128.

[12] Possell M, Bell TL. The influence of fuel moisture content on the combustion of Eucalyptus foliage. Int J Wildland Fire 2013;22:343–52. https://doi.org/10.1071/WF12077.

[13] Leroy V, Cancellieri D, Leoni E. Relation between forest fuels composition and energy emitted during their thermal degradation. J Therm Anal Calorim 2009;96: 293. https://doi.org/10.1007/s10973-008-9587-9.

[14] de Rivera JD, Davies GM, Jahn W. Flammability and the heat of combustion of natural fuels: a review. Combust Sci Technol 2012;184:224–42. https://doi.org/10.1080/00102202.2011.630332.

[15] Weise DR, White RH, Beall FC, Etlinger M. Use of the cone calorimeter to detect seasonal differences in selected combustion characteristics of ornamental vegetation*. Int J Wildland Fire 2005;14:321–38. https://doi.org/10.1071/WF04035.

[16] Qi Y, Jolly WM, Dennison PE, Kropp RC. Seasonal relationships between foliar moisture content, heat content and biochemistry of lodgepole line and big sagebrush foliage. Int J Wildland Fire 2016;25:574–8. https://doi.org/10.1071/WF15156.

[17] Rothermel RC, Philpot CW. Predicting changes in chaparral flammability. J For 1973;71(10):640–3.

[18] Hough WA, Albini FA. Predicting fire behavior in palmetto-gallberry fuel complexes. Research Paper SE-RP-174Asheville, NC: USDA-Forest Service, Southeastern Forest Experiment Station 48 p 1978;174:1–48.

[19] Albini FA. Thermochemical properties of flame gases from fine wildland fuels. Res Pap INT-RP-243 Ogden, UT: US Department of Agriculture, Forest Service, Intermountain Forest and Range Experiment Station 42 p 1979;243.

[20] Babrauskas V. Effective heat of combustion for flaming combustion of conifers. Can J For Res 2006;36:659–63. https://doi.org/10.1139/x05-253.

[21] Weise DR, Fletcher TH, Cole W, Mahalingam S, Zhou X, Sun L, et al. Fire behavior in chaparral–Evaluating flame models with laboratory data. Combust Flame 2018; 191:500–12. https://doi.org/10.1016/j.combustflame.2018.02.012.

[22] Stitt F, Kennedy EK. Specific heats of dehydrated vegetables and egg powder. J Food Sci 1945;10:426–36. https://doi.org/10.1111/j.1365-2621.1945.tb16188.x.

[23] Amini E, Safdari M-S, Weise DR, Fletcher TH. Pyrolysis kinetics of live and dead wildland vegetation from the Southern United States. J Anal Appl Pyrol 2019;142: 104613. https://doi.org/10.1016/j.jaap.2019.05.002.

[24] Michaletz ST, Johnson EA. A heat transfer model of crown scorch in forest fires. Can J For Res 2006;36:2839–51. https://doi.org/10.1139/x06-158.

[25] Jayalakshmy MS, Philip J. Thermophysical properties of plant leaves and their influence on the environment temperature. Int J Thermophys 2010;31:2295–304. https://doi.org/10.1007/s10765-010-0877-7.

[26] Glass SV, Zelinka SL. Moisture relations and physical properties of wood. Wood handbook : wood as an engineering material: chapter 4. Centennial ed., Madison, WI, USA: Forest Products Laboratory, USDA Forest Service; 2010, p. 4.1-4.19.

[27] Dupont C, Chiriac R, Gauthier G, Toche F. Heat capacity measurements of various biomass types and pyrolysis residues. Fuel 2014;115:644–51. https://doi.org/10.1016/j.fuel.2013.07.086.

[28] Pooley LI, Abu-Bakar AS, Cran MJ, Wadhwani R, Moinuddin KAM. Measurements of specific heat capacity of common building materials at elevated temperatures: a comparison of DSC and HDA. J Therm Anal Calorim 2020;141:1279–89. https://doi.org/10.1007/s10973-019-09124-5.

[29] Thybring EE. Explaining the heat capacity of wood constituents by molecular vibrations. J Mater Sci 2014;49:1317–27. https://doi.org/10.1007/s10853-013-7815-6.

[30] Cho J, Davis JM, Huber GW. The intrinsic kinetics and heats of reactions for cellulose pyrolysis and char formation. ChemSusChem 2010;3:1162–5. https://doi.org/10.1002/cssc.201000119.

[31] Werner K, Pommer L, Broström M. Thermal decomposition of hemicelluloses. J Anal Appl Pyrol 2014;110:130–7. https://doi.org/10.1016/j.jaap.2014.08.013.

[32] Dietenberger MA, Boardman CR, Weise DR. Heats for combustion, capacities, and evaporation of fresh leaves, and their relationships to leaf compositions. In: Proceedings, 6th International Fire Behavior and Fuels Conference Missoula, MT: International Association of Wildland Fire 6 p 2019.

[33] Matt FJ, Dietenberger MA, Weise DR. Summative and ultimate analysis of live leaves from southern u.s. forest plants for use in fire modeling. Energy Fuels 2020; 34:4703–20. https://doi.org/10.1021/acs.energyfuels.9b04107.

[34] USDA. PLANTS Database 2020. https://plants.sc.egov.usda.gov/java/ (accessed July 29, 2020).

[35] Radford AE, Ahles HE, Bell CR. Manual of the vascular flora of the carolinas. Chapel Hill, NC: The University of North Carolina Press; 1968.

[36] Thomas LC, Modulated DSC. Paper #9: measurement of accurate heat capacity values. New Castle, DE, USA: TA Instruments; 2005.

[37] Danley RL. New modulated DSC measurement technique. Thermochim Acta 2003; 402:91–8. https://doi.org/10.1016/S0040-6031(02)00541-5.

[38] Lin Y-C, Cho J, Tompsett GA, Westmoreland PR, Huber GW. Kinetics and mechanism of cellulose pyrolysis. J Phys Chem C 2009;113:20097–107. https://doi.org/10.1021/jp906702p.

[39] Anca-Couce A, Tsekos C, Retschitzegger S, Zimbardi F, Funke A, Banks S, et al. Biomass pyrolysis TGA assessment with an international round robin. Fuel 2020; 276:118002. https://doi.org/10.1016/j.fuel.2020.118002.

[40] Butland ATD, Maddison RJ. The specific heat of graphite: an evaluation of measurements. J Nucl Mater 1973;49:45–56. https://doi.org/10.1016/0022-3115(73)90060-3.

[41] Xin S, Yang H, Chen Y, Yang M, Chen L, Wang X, et al. Chemical structure evolution of char during the pyrolysis of cellulose. J Anal Appl Pyrol 2015;116: 263–71. https://doi.org/10.1016/j.jaap.2015.09.002.

[42] Tang WK, Eickner HW. Effect of inorganic salts on pyrolysis of wood, cellulose, and lignin determined by differential thermal analysis. Madison, WI, USA: U.S. Department of Agriculture, Forest Service, Forest Products Laboratory; 1968.

[43] Nassar MM, MacKay GDM. Mechanism of thermal decomposition of lignin. Wood Fiber Sci 1984;16:441–53.

[44] Faleeva JM, Sinelshchikov VA, Sytchev GA, Zaichenko VM. Exothermic effect during torrefaction. J Phys: Conf Ser 2018;946:012033. https://doi.org/10.1088/1742-6596/946/1/012033.

[45] Yang H, Yan R, Chen H, Lee DH, Zheng C. Characteristics of hemicellulose, cellulose and lignin pyrolysis. Fuel 2007;86:1781–8. https://doi.org/10.1016/j.fuel.2006.12.013.

[46] Anca-Couce A, Scharler R. Modelling heat of reaction in biomass pyrolysis with detailed reaction schemes. Fuel 2017;206:572–9. https://doi.org/10.1016/j.fuel.2017.06.011.

[47] Hatakeyama T, Nakamura K, Hatakeyama H. Studies on heat capacity of cellulose and lignin by differential scanning calorimetry. Polymer 1982;23:1801–4. https://doi.org/10.1016/0032-3861(82)90125-2.

[48] Blokhin AV, Voitkevich OV, Kabo GJ, Paulechka YU, Shishonok MV, Kabo AG, et al. Thermodynamic properties of plant biomass components. heat capacity, combustion energy, and gasification equilibria of cellulose. J Chem Eng Data 2011; 56:3523–31. https://doi.org/10.1021/je200270t.

[49] Ribeiro da Silva MAV, Ribeiro da Silva MDMC, Lobo Ferreira AIMC, Shi Q, Woodfield BF, Goldberg RN. Thermochemistry of α-D-xylose(cr). J Chem Thermodyn 2013;58:20–8. https://doi.org/10.1016/j.jct.2012.09.028.

[50] Voitkevich OV, Kabo GJ, Blokhin AV, Paulechka YU, Shishonok MV. Thermodynamic Properties of Plant Biomass Components. Heat Capacity, Combustion Energy, and Gasification Equilibria of Lignin. J Chem Eng Data 2012; 57:1903–9. https://doi.org/10.1021/je2012814.

[51] Rudtsch S. Uncertainty of heat capacity measurements with differential scanning calorimeters. Thermochim Acta 2002;382:17–25. https://doi.org/10.1016/S0040-6031(01)00730-4.